ILASS-Americas 31st Annual Conference on Liquid Atomization and Spray Systems, May 2021

Multi-component transcritical flow simulation using in situ adaptive tabulation of vapor-liquid equilibrium solutions

Hongyuan Zhang[*], Suo Yang[†]
Department of Mechanical Engineering
University of Minnesota – Twin Cities
Minneapolis, MN 55455 USA

Abstract

The studies of transcritical and supercritical injection have attracted much interest in the past 30 years. However, most of them were mainly concentrated on the single-component system, whose critical point is a constant value. To capture the thermophysical properties of multicomponent, a phase equilibrium solver is needed, which is also called a vapor-liquid equilibrium (VLE) solver. But VLE solver increases the computation cost significantly. Tabulation methods can be used to store the solution to avoids a mass of redundant computation. However, the size of a table increases exponentially with respect to the number of components. When the number of species is greater than 3, the size of a table far exceeds the limit of RAM in today's computers. In this research, an online tabulation method based on *In Situ* Adaptive Tabulation (ISAT) is developed to accelerate the computation of multicomponent fluid. Accuracy and efficiency are analyzed and discussed. The CFD solver used in this research is based on the Pressure-Implicit with Splitting of Operators (PISO) method. Peng-Robinson equation of state is used in phase equilibrium.

[*]Ph.D Candidate.
[†]Richard & Barbara Nelson Assistant Professor, suoyang@umn.edu (Corresponding Author).

Introduction

The demand for high-performance combustors increases the chamber pressure continuously, making the working condition of some high-pressure combustors overlap with the supercritical region of fuel and/or oxidizer. The injection and mixing process is very different between subcritical and supercritical conditions [1, 2], which could affect the cold ignition in combustors. To understand the subcritical and supercritical mixing process, a simulation tool is needed. Since the supercritical region is far from the ideal gas region, the real-gas effect needs to be considered to capture correct behavior. In addition, transcritical and supercritical fluid behavior can be peculiar because of the considerable variation of thermophysical properties such as density and specific heat near the critical point. As a result, the Computational Fluid Dynamics (CFD) modeling of supercritical flows is very challenging. Since small changes in temperature and pressure can significantly affect a fluid's structure near the critical point, local properties are very important. Furthermore, a supercritical fluid lacks surface tension, which means the modeling transcritical flow needs to capture the surface tension change when the fluid goes across the phase boundary. This makes simulation of transcritical flow more challenging than supercritical flow.

The studies of transcritical and supercritical injection and mixing have attracted much interest in the past 30 years. However, most of them were mainly concentrated on the single-component system, whose critical point is a constant value. As long as the fluid exceeds its critical point, it goes into the supercritical state, and the classical "dense-fluid" approach is used with the assumption of a single-phase [3]. Since the real mixture critical pressure could be significantly higher than the critical pressure of each component [4], the accurate mixture critical point needs to be obtained.

Recently, some works focus on multicomponent transcritical flow simulation, capturing the phase separation at high pressure. Most works use the vapor-liquid equilibrium (VLE) theory to capture phase separation. Yao, et al. developed a fluids solver based on VLE to investigate the impact of diffusion models of a laminar counter-flow flame at trans and supercritical conditions [5]. In Ray's work, VLE theory is used to understand fuel droplets evaporation at high pressures [6]. A similar framework is also used in P. Tudisco's works to understand the effect of Lewis number [7].

However, all these works are limited to two-component transcritical flow simulation. The VLE solver brings a huge amount of computation cost, limiting the simulation of complex geometry and multicomponent flow. To reduce the computational cost, Tudisco, et al. interpolates the thermodynamic properties from cell-centers to cell-interfaces [8], but still can not accelerate the computation at cell-centers. Yi, et al. used a tabulation method to avoid computing of VLE model. However, the table size grows exponentially (table size M^N, M is the number of the grid in the table; N is the number of components). For a flow with four components, table size will need several Terabytes, making this method completely unsuitable for combustion and many other practical problems.

In this work, we coupled *In Situ* Adaptive Tabulation with the transcritical fluid solver to accelerate computation. The ISAT method constructs the table during the computation. It only stores the necessary data, which only requires a small amount of computer storage and achieves high computational speed [9]. The new solver with ISAT gained a great computational speed improvement.

Numerical Modeling

Models of thermodynamic and transport properties

This study uses VLE solvers to capture the phase change and determine the multicomponent mixture's critical point in the transcritical flow. VLE describes the phase equilibrium between liquid and vapor phases. Solving the set of VLE equations gives the phase fraction and compositions in the two phases. If the gas mole fraction (i.e., the mole fraction of vapor phase) is equal to 1 or 0, then the system is in a purely gaseous or liquid phase, respectively. If the system falls into the two-phase region, the gas fraction will be between 0 and 1, and equilibrium between vapor and liquid will be observed. Suppose, at certain conditions, thermodynamic properties become identical between liquid and gas. In that case, it indicates the occurrence of a transcritical transition from a subcritical state to a supercritical state (which could be a liquid-like or gas-like state). The fluid solver that we implemented is coupled with isobaric and isenthalpic (PHn) flash solver[10]. PHn flash and almost all other VLE solvers are developed based on the TPn flash. Specifically, PHn flash solves the VLE equation set at given enthalpy (H) rather than temperature. The TPn flash is the most basic VLE solver, which solves the set of VLE equations at a given temperature (T), pressure (P), and mole fraction of each component (n) in the system.

Isothermal and isobaric (TPn) flash:

VLE is governed by fugacity equality Eq. (1)

and Rachford-Rice equation [11] Eq. (2), which is an additional constraint to the equilibrium solver as used in [12] and obtained from the conservation of each component.

$$f_{i,l}/f_{i,g} = 1 \tag{1}$$

$$\sum_{i=1}^{N} \left\{ z_i \left(1 - K_i\right) \Big/ \left[1 + \left(K_i - 1\right) \psi_g\right] \right\} = 0 \tag{2}$$

$$K_i = y_i/x_i \tag{3}$$

$$\sum_{i=1}^{N} x_i = \sum_{i=1}^{N} y_i = 1 \tag{4}$$

where $f_{i,p}$ is the fugacity of component i in phase p ($p = l$: liquid; $p = g$: gas), x_i is the mole fraction of component i in liquid phase, y_i is the mole fraction of component i in gas phase, z_i is the mole fraction of component i in the feed (i.e., the whole mixture including both gas phase and liquid phase), ψ_g is the gas mole fraction, K_i is the equilibrium constant of component i.

The real fluid properties are described using the Peng-Robinson equation of state (PR-EOS) [13] as:

$$P = \frac{RT}{V - b} - \frac{a}{V\left(V + b\right) + b\left(V - b\right)} \tag{5}$$

where P, R, T and V are pressure, gas constant, temperature, and specific volume respectively. For single-component fluid, the PR-EOS parameters are given by

$$a = 0.45724 \frac{R^2 T_c^2}{p_c} \hat{a}, \tag{6}$$

$$b = 0.07780 \frac{RT_c}{p_c}, \tag{7}$$

$$\hat{a} = \left(1 + \kappa \left(1 - \left(T_r\right)^{1/2}\right)\right)^2, \tag{8}$$

$$\kappa = 0.37464 + 1.54226\omega - 0.26992\omega^2 \tag{9}$$

where subscript "c" means critical value, subscript "r" means the reduced value (e.g., $T_r = T/T_c$), ω is acentric factor.

The mixture PR-EOS parameters are calculated from the corresponding single component coefficients a_i and b_i using the mixing rule [14]:

$$a = \sum_i \sum_j \chi_i \chi_j (1 - b_{ij}) \sqrt{a_i a_j} \tag{10}$$

$$b = \sum_i \chi_i b_i \tag{11}$$

where χ_i is the mole fraction of component i (for liquid, $\chi_i = x_i$; for gas phase, $\chi_i = y_i$), b_{ij} is a binary interaction parameter.

The liquid phase and the gas phase are described by two multicomponent PR-EOS, respectively. The specific volume of each phase, V_p, is solved from PR-EOS. The compressibility factor of each phase ($Z = PV/RT$) can also be obtained from this.

The fugacity formula of PR-EOS is shown below [15]:

$$\begin{aligned} f_i = & P\chi_i \exp\Bigg[\frac{B_i}{B_{mix}}(Z-1) - ln(Z - B_{mix}) \\ & - \frac{A_{mix}}{2\sqrt{2}B_{mix}} \left(\frac{2\sum_j x_j A_j}{A_{mix}} - \frac{B_i}{B_{mix}}\right) \\ & \times ln\left(\frac{Z + (1+\sqrt{2})B_{mix}}{Z + (1-\sqrt{2})B_{mix}}\right)\Bigg] \end{aligned} \tag{12}$$

where χ_i is the mole fraction of component i (for liquid, $\chi_i = x_i$; for gas phase, $\chi_i = y_i$),

$$A_i = \frac{a_i p}{R^2 T^2}, \tag{13}$$

$$B_i = \frac{b_i p}{RT}, \tag{14}$$

$$A_{mix} = \sum_i \sum_j x_i x_j (1 - b_{ij}) \sqrt{A_i A_j}, \tag{15}$$

$$B_{mix} = \sum_i x_i B_i \tag{16}$$

The equation set Eq. (1-16) is solved based on Newton iteration method. The flow chart of the TPn flash is shown in Fig. 1. The initial guess is obtained using Wilson Equation [16]:

$$K_i = e^{5.373(1+\omega_i)(1-1/T_{r,i})}/P_{r,i} \tag{17}$$

where ω_i is the acentric factor of component i; $T_{r,i}$ and $P_{r,i}$ are the reduced temperature and reduced pressure of component i, respectively. Then, solving Rachford-Rice equation (i.e., Eq. 2) using Newton iteration method to get ψ_g. x_i and y_i can be obtained from Eqs. (3) and (4). The next step is to evaluate fugacity using the Eq. (12-16), and examine whether fugacity equilibrium (i.e., $f_{i,l} = f_{i,g}$) has been reached. If not, update K_i by $K_i = K_i \times f_{i,l}/f_{i,g}$ and go back to solve Rachford-Rice equation. When the error is less than a tolerance (i.e., the Newton iteration is converged), the solver will break the loop and output the solution.

Isobaric and Isenthalpic (PHn) flash:

In this work, the fluid solver uses Pressure-Implicit with Splitting of Operators (PISO) method, which directly updates pressure, enthalpy, and mass fraction of every component from the fluid governing equation. The equilibrium temperature T_{eq} is determined using PHn flash to evaluate other thermodynamic and transport properties. the corresponding

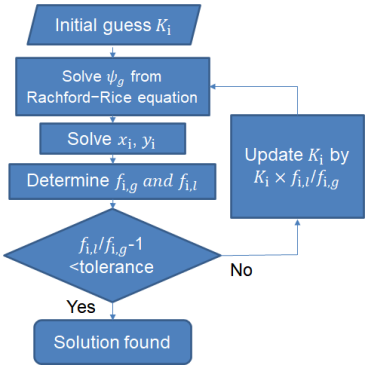

Figure 1. Flow chart of the TPn flash solver.

objective function is expressed as

$$F_h = (h^* - h)/h^* \tag{18}$$

where h^* is the specific mixture enthalpy obtained from the fluid solver. The enthalpy of each phase p is calculated as

$$h_p(T,P) = h_{p,ideal}(T,p) + h_{p,dep}(T,p) \tag{19}$$

where h_{ideal} is the enthalpy of component i in ideal gas state, which is evaluated by JANAF polynomials; and h_{dep} is the departure enthalpy, calculated as:

$$h_{p,dep}(T,P) = RT(Z_p - 1) + \frac{T\frac{da_p}{dT} - a_p}{2\sqrt{2}b_p} ln \frac{Z_p + (1+\sqrt{2})B_{p,mix}}{Z_p + (1-\sqrt{2})B_{p,mix}} \tag{20}$$

where a_p, b_p and $B_{p,mix}$ are PR-EOS parameters of phase p defined in Eq. (10,11,16).

The enthalpy of two-phase mixture is calculated as

$$h = \psi_g h_g + (1-\psi_g) h_l \tag{21}$$

The equation is solved by the Newton iteration method. Equilibrium temperature T_{eq} is updated in PHn flash iteratively as

$$T_n = T_{n-1} + (h^* - h(T_{n-1}, P)) \Big/ C_{p,mix}(T_{n-1}, P) \tag{22}$$

$$C_{p,mix} = \frac{h(T+\Delta T, P) - h(T,P)}{\Delta T} \tag{23}$$

Transport properties:

The dense fluid formula [17] is used to evaluate the dynamic viscosity and thermal conductivity under transcritical conditions. This method gives accurate estimations of viscosity and thermal conductivity of polar, non-polar and associating pure fluids and mixtures. Its dynamic viscosity and thermal conductivity have a similar formula:

$$\lambda = \lambda_0 \lambda^* + \lambda_p \tag{24}$$

where λ represents dynamic viscosity or thermal conductivity. λ_0 is the gas property at low pressures. λ^* and λ_p are high-pressure corrections. At high pressures, λ_p is the major contributing term comparing to $\lambda_0\lambda^*$. On the other hand, at low pressures, λ^* is approaching unity, and the λ_p term is negligible such that Eq. 24 reduces to λ_0. Hence, the transition between subcritical and supercritical is smoothly described by the model.

In Situ Adaptive Tabulation (ISAT)

In situ adaptive tabulation method is introduced by Pope [9] to reduce the computational cost of detailed chemistry calculations. Compared to the traditional tabulation methods, which generate a table before computation, ISAT dynamically constructs a table during the computation, which enables us to store necessary records to reduce the table size. Although ISAT still needs to calculate the target function, most queries can be directly retrieved by linear approximation. In addition, ISAT not only balances time and space cost but also provides good error control. Hence, it is a good choice to accelerate the PHn flash solver.

The PISO based fluid solver directly updates pressure P, enthalpy h, and mass mole fraction of every component Y_m from the governing equation, and require thermodynamic model to evaluate $\phi = P/\rho$, temperature T, and gas mole fraction ψ_g, which can be solved by PHn flash solver. The relation between the given condition and solution of PHn flash solver can be denote as a function,

$$\boldsymbol{y} = \boldsymbol{F}(\boldsymbol{x}), \mathbf{x} = (\mathbf{Y}, P, h), \mathbf{y} = (T, \phi, \psi_g)$$

For every record in the table, it contains $(\mathbf{x}_0, \mathbf{y}_0, \frac{\partial \mathbf{F}}{\partial \mathbf{x}}\big|_{\mathbf{x}_0}, \mathbf{M})$

The gradient, $\frac{\partial \mathbf{F}}{\partial \mathbf{x}}\big|_{\mathbf{x}_0}$, is evaluated numerically and used for local linear approximation,

$$\mathbf{y}_{linear} = \mathbf{y}_0 + \frac{\partial \mathbf{F}}{\partial \mathbf{x}}\bigg|_{\mathbf{x}_0} \cdot (\mathbf{x} - \mathbf{x}_0)$$

The matrix $\mathbf{M}$ is used to define the region of accuracy, in which the local error ϵ does not exceed the tolerance ϵ_{tol}. The region of accuracy is defined by inequality

$$(\mathbf{x}-\mathbf{x}_0)^T \mathbf{M} (\mathbf{x}-\mathbf{x}_0) \leq 1$$

The point satisfying this inequality is a hyper-ellipsoid. So, the region of accuracy is also called ellipsoid of accuracy (EOA).

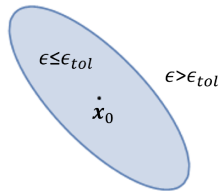

Figure 2. Sketch of region of accuracy

For the initial setting, the linear term is considered as the error. So, the initial $\mathbf{M}$ can be set as

$$\mathbf{M} = \left(\frac{\partial \mathbf{F}}{\partial \mathbf{x}}\bigg|_{\mathbf{x}_0} \right)^T \left(\frac{\partial \mathbf{F}}{\partial \mathbf{x}}\bigg|_{\mathbf{x}_0} \right) / \epsilon_{tol}^2$$

.

For the first query, a new record is calculated and added to the table. For subsequent queries ($\mathbf{x}_{new}$), the closest record ($\mathbf{x}_0, \mathbf{y}_0, \frac{\partial \mathbf{F}}{\partial \mathbf{x}}\big|_{\mathbf{x}_0}, \mathbf{M}$) is find out.

(1). **Retrieve**. If $\mathbf{x}_{new}$ is in the EOA of the record, then the linear approximation, $\mathbf{y}_{linear}$, is returned.

(2). **Growth**. If retrieve failed, then $\mathbf{y}_{new} = \mathbf{F}(\mathbf{x}_{new})$ is calculated. If $|\mathbf{y}_{new} - \mathbf{y}_{linear}| \leq \epsilon_{tol}$, the EOA is grown. The new EOA is the smallest ellipsoid covering old EOA and $\mathbf{x}_{new}$. $\mathbf{y}_{new}$ is returned.

(3). **Addition**. If growth also failed, then a new record is added to the table, and $\mathbf{y}_{new}$ is returned.

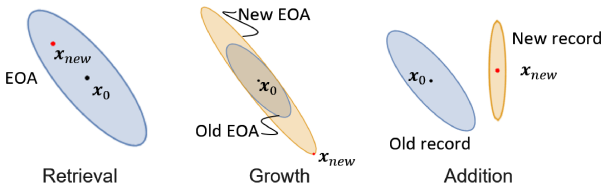

Figure 3. Sketch showing the algorithm of ISAT method

CFD simulation framework

In this investigation, a transcritical multiphase CFD solver is developed by coupling a CFD solver with the TPn flash VLE solver. The CFD solver is based on multicomponent transport equations, including the continuity equation, mixture momentum equations, mixture specific internal enthalpy equation, and balance equations for distinct components in the mixture as follows:

$$\frac{\partial \rho}{\partial t} + \frac{\partial \rho u_i}{\partial x_i} = 0 \tag{25}$$

$$\frac{\partial \rho u_i}{\partial t} + \frac{\partial \rho u_i u_j}{\partial x_j} = \frac{\partial P}{\partial x_i} + \frac{\partial \tau_{ij}}{\partial x_j} \tag{26}$$

$$\frac{\partial \rho (h+K) - P}{\partial t} + \frac{\partial \rho u_i (h+K)}{\partial x_i} = -\frac{\partial q_i}{\partial x_i} + \frac{\partial \tau_{ij} u_j}{\partial x_i} \tag{27}$$

$$\frac{\partial \rho Y_m}{\partial t} + \frac{\partial \rho Y_m u_j}{\partial x_i} = \frac{\partial}{\partial x_j}\left(\rho D \sum_m h_m \frac{\partial Y_m}{\partial x_j} \right) \tag{28}$$

where ρ and h are mixture density and internal enthalpy, respectively, and Y_m is mass fraction of component m. Pressure P is obtained from the EOS in a general form:

$$\rho = \phi P \tag{29}$$

in which the specific form of ϕ is depending on whether VLE is used and which EOS are used (e.g., ideal gas EOS and PR-EOS).

The CFD solver is capable of solving subsonic and transonic flows with and without reactions. It uses Pressure-Implicit with Splitting of Operators (PISO) method [18] for solving the governing equations, which includes a predictor step and multiple corrector steps. In PISO, the momentum equations (Eq. 26) are linearly discretized into the following matrix form:

$$Au + \sum_{ne} A_{ne} u_{ne} = S + \nabla P \tag{30}$$

where u_{ne} is the velocity of a neighbor gird ne, A_{ne} and A are the corresponding coefficients, and S is a constant term. Rearranging Eq. (30) gives the following form:

$$u = H^* - \frac{\nabla P}{A} \tag{31}$$

$$H^* = \frac{S - \sum_{ne} A_{ne} u_{ne}}{A} \tag{32}$$

By substituting EOS (Eq. 29) and Eq. (31) into the continuity equation (Eq. 25), we can get:

$$\text{Subsonic: } \frac{\partial \phi P}{\partial t} + \nabla \cdot \left[\rho \left(H^* - \frac{\nabla P}{A} \right) \right] = 0 \tag{33}$$

$$\text{Transonic: } \frac{\partial \phi P}{\partial t} + \nabla \cdot (\phi P H^*) - \nabla \cdot \left(\rho \frac{\nabla P}{A} \right) = 0 \tag{34}$$

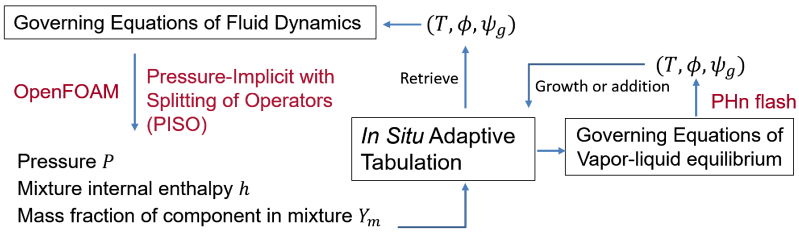

Figure 4. Flow chart of the VLE-based CFD solver.

Eq. (34) is obtained by substituting EOS (Eqs. 29) into the second term of Eq. (33). With this change, the solver is able to capture the compressibility better. Hence, Eqs. (33) and (34) are used to solve subsonic and transonic flows respectively.

At each step, the CFD solver updates fluid properties, including mixture density ρ, mixture enthalpy h, and mass fraction Y_m, which are enough to determine the thermal equilibrium state. In the simulation, the partial equilibrium state, rather than the global equilibrium, is assumed to be achieved immediately at every grid point. This partial equilibrium state can be obtained from the VLE solver. Hence, by solving PHn VLE at given $(\mathbf{Y}, P, h)$, equilibrium temperature T, ϕ, and ψ_g is updated for the next time step which is shown in Fig. 4. Due to the high computational cost of VLE calculation, ISAT is used to store the VLE solution calculated by PHn flash to avoid repeated computation.

Result and Analysis

Fluid simulation and performance of ISAT: 1D shock tube

In order to show the effect of the VLE solver and test the performance of ISAT, a shock tube case of a CO_2/H_2O mixture is tested, which includes a compression shock wave and an expansion wave. The initial condition of the test case is shown in Table 1. In the simulations, to show the importance of EOS and VLE models in CFD simulations, three models are used and compared: ideal gas model, real fluid model (PR-EOS) without phase change (i.e., no VLE), and real fluid model (PR-EOS) with phase change (i.e., VLE). From the pressure plot in Fig. 5(a), it is apparent that expansion wave in PR-EOS with VLE model propagates slower, which is due to lower sound speed. In the isentropic process, the pressure change is reduced by phase change. Hence, sound speed $c = \sqrt{\left(\frac{\partial p}{\partial \rho}\right)_s}$ is smaller. However, the mixture in the compression shock wave is in a purely gaseous phase due to the higher temperature. Thus, the shock wave speed is not affected by phase change, and the post-compressor mixture should be in a purely gaseous phase. In Fig. 5(b), because phase change is taken into account, latent heat is released when vapor partially condenses, which reduces the temperature change and makes PR-EOS with VLE have the highest temperature. In Fig. 5(c), the three models show an evident difference in density prediction. Specifically, compared to the real fluid models (PR-EOS), the ideal gas model underestimates the gas density. The effect of the phase change (i.e., VLE) increases the temperature in the expansion wave reduces the density there. The red dashed line shows the vapor mole fraction predicted by the real fluid model with phase change (i.e., VLE) at different positions, which indicates that the mixture is partially condensed after the expansion wave. A sharp bend (point A) in the density line only exists in the PR-EOS model with VLE, which corresponds to the location where the mixture starts to condense partially. The Mach number of this shock tube is 1.25, which indicates that the transonic version of the PISO method is able to handle the compressibility of relatively large Mach number flows.

	P (bar)	T (K)	x_{CO_2}	x_{H_2O}
left	230	500	0.7	0.3
right	100	550	0.7	0.3

Table 1. Initial condition for a shock tube with CO_2/H_2O mixture.

This shock tube simulation is also used for the ISAT performance test. The shock tube (0.1mm) is evenly divided into 1000 grids. The simulation is run to $5 \times 10^{-8} s$. The simulation is run serially on a PC equipped with an Intel Core i7-8700K CPU. In Tab. 2. The running time of the VLE model is about 40 times that of the ideal gas model, which shows that the VLE solver introduces a huge amount of computational cost.

First, to understand the accuracy of the ISAT

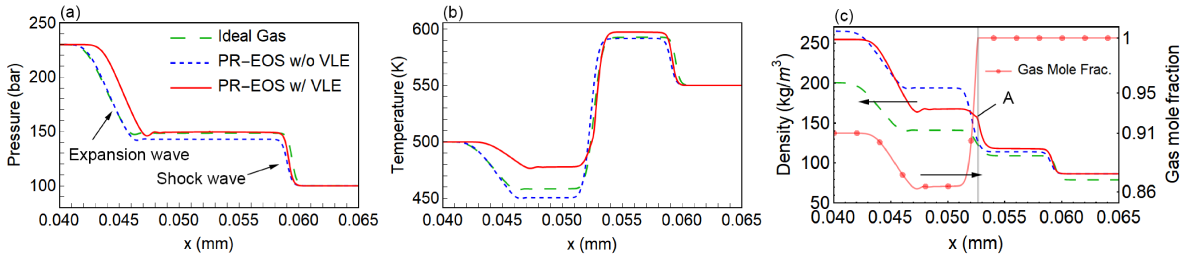

Figure 5. Simulation results of a shock tube with CO_2/H_2O mixture, at $t = 2 \times 10^{-8}s$: (a) pressure; (b) temperature; (c) density (solid lines) and gas mole fraction (dashed line).

	Ideal gas	VLE
Times (s)	4s	165s

Table 2. Running time for a shock tube with CO_2/H_2O mixture.

method, two simulations are conducted. The first one use $\epsilon_{tol} = \epsilon_{tol_0} = (1K, 1 \times 10^{-6}m^2/s^2, 1 \times 10^{-2})$, which is chosen based on the magnitude of $\mathbf{y} = (T, \phi, \psi_g)$. The second one used a smaller tolerance to control the error $\epsilon_{tol} = \epsilon_{tol_0}$. Fig. 6(a-b) shows that in the first simulation, the tolerance is too large, that linear approximation is not enough to obtain an accurate result. At $x = 0.04mm$, the pressure and gas mode fraction results give a significant deviation. The second simulation, in Fig. 6(c-d), shows with smaller tolerance could capture the shock wave and expansion wave very well.

Then, we conducted a series of simulations to find out a proper tolerance. The tolerance is $\epsilon_{tol} = k\epsilon_{tol_0}$. In Fig. 7 (a) and Fig. 7 (b), we can see with the increase of the threshold ϵ_{tol}, the error of pressure and gas mole fraction presents an overall trend of increase. The error of the points in the red circle is acceptable for this shock tube simulation. Fig. 7 (c) shows that the running time decreases as the threshold increases. A running time of 12s 14s is needed to obtain a result of acceptable accuracy. Compared to the case without the ISAT method (Running time 165s), the ISAT method enables the simulation to run about 12 times faster. This shock tube only contains two components (CO2 and H2O). We believe we can obtain an even better speed-up factor for simulation with a larger number of components.

Conclusion

We implemented a vapor-liquid equilibrium (VLE) solver (PHn flash) and coupled PHn flash

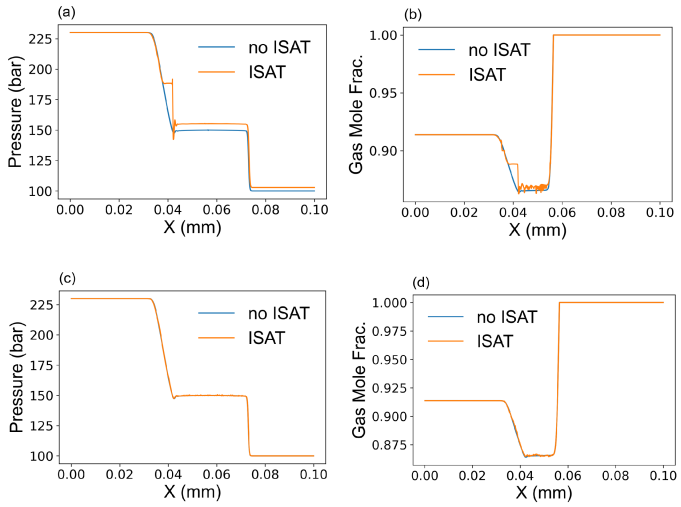

Figure 6. Comparison between result with ISAT and w/o ISAT: (a) and (b) $\epsilon_{tol} = \epsilon_{tol_0} = (1K, 1 \times 10^{-6}m^2/s^2, 1 \times 10^{-2})$; (c) and (d) $\epsilon_{tol} = 0.05\epsilon_{tol_0}$; (a) and (c) pressure plot; (b) and (d) gas mole fraction plot.

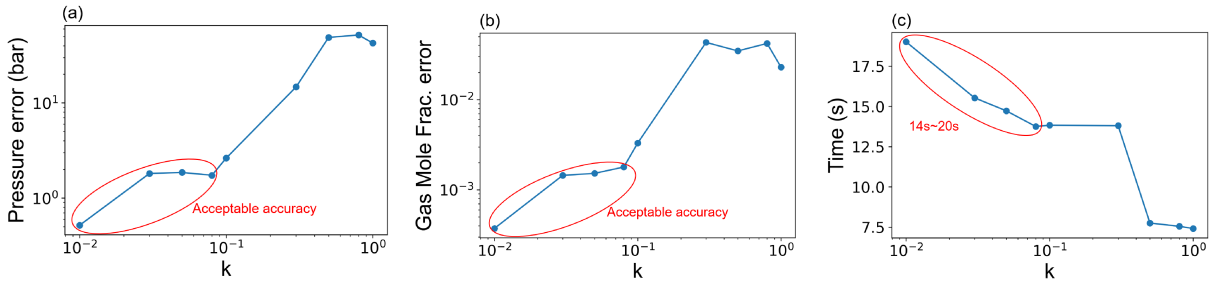

Figure 7. The effect of tolerance on ISAT performance. k versus (a) pressure error, (b) gas mole faction error, (c) running time.

solver with a computational fluid dynamics (CFD) solver to capture the mixing and phase separation processes of mixtures. The ISAT method is used to store the solution of PHn flash to reduce the huge computation cost brought by vapor-liquid equilibrium (VLE) solvers A series of shock tube simulations are conducted to determine a tolerance that controls error within the acceptable range and has an excellent speed-up factor. Finally, by choosing a proper tolerance, we obtain a speed-up factor of above 12. This speed-up factor is obtained from a two-component flow. Since the VLE solver of a larger number of components requires more computation resources, we anticipate getting an even better speed-up factor for simulation with more components.

Acknowledgments

S. Yang gratefully acknowledges the faculty start-up funding from the University of Minnesota and the grant support from NSF CBET 2023932. H. Zhang gratefully acknowledges the support from the 3M Science and Technology Doctoral Fellowship and UMII MnDRIVE Graduate Assistantship Award. Part of the computational resources was provided by the Minnesota Supercomputing Institute (MSI).

References

[1] B Chehroudi, D Talley, and E Coy. *37th Aerospace Sciences Meeting and Exhibit*, p. 206, 1999.

[2] W Mayer and Joshua J Smith. *Liquid Rocket Thrust Chambers: Aspect of Modeling, Analysis, and Design, Progress in Astronautics and Aeronautics*, 200:339–368, 2004.

[3] Vigor Yang. *Proceedings of the Combustion Institute*, 28(1):925–942, 2000.

[4] PH Van Konynenburg and RL Scott. *Philosophical Transactions of the Royal Society of London. Series A, Mathematical and Physical Sciences*, 298(1442):495–540, 1980.

[5] Matthew X Yao, Jean-Pierre Hickey, Peter C Ma, and Matthias Ihme. *Combustion and Flame*, 210:302–314, 2019.

[6] Saroj Ray, Vasudevan Raghavan, and George Gogos. *International Journal of Multiphase Flow*, 111:294–309, 2019.

[7] P Tudisco and S Menon. *Physics of Fluids*, 32(11):112111, 2020.

[8] Principio Tudisco and Suresh Menon. *Flow, Turbulence and Combustion*, 104(2):693–724, 2020.

[9] Stephen B Pope. *Combustion Theory and Modelling*, 1(1):41–63, 1997.

[10] Michael L Michelsen. *Fluid phase equilibria*, 33(1-2):13–27, 1987.

[11] HH Rachford Jr, JD Rice, et al. *Journal of Petroleum Technology*, 4(10):19–3, 1952.

[12] Sanjoy Saha and John J Carroll. *Fluid phase equilibria*, 138(1-2):23–41, 1997.

[13] Ding-Yu Peng and Donald B Robinson. *Industrial & Engineering Chemistry Fundamentals*, 15(1):59–64, 1976.

[14] Robert C Reid, John M Prausnitz, and Thomas K Sherwood. *The Properties of Liquids and Gases.(Stichworte Teil 2)*. McGraw-Hill, 1977.

[15] Ping Yi, Songzhi Yang, Chaouki Habchi, and Rafael Lugo. *Physics of Fluids*, 31(2):026102, 2019.

[16] Grant M Wilson. *Journal of the American Chemical Society*, 86(2):127–130, 1964.

[17] Ting Horng Chung, Mohammad Ajlan, Lloyd L Lee, and Kenneth E Starling. *Industrial & engineering chemistry research*, 27(4):671–679, 1988.

[18] Fabian Peng Kärrholm. *Department of Applied Mechanics, Chalmers University of Technology: Goteborg, Sweden*, 2006.